HS 1804 + 6753: a new eclipsing CV above the period gap*

H. Fiedler, H. Barwig, and K.H. Mantel

Universitäts-Sternwarte, Scheinerstr. 1, D-81679 München, Germany

Abstract. We present spectroscopic and photometric observations of the cataclysmic variable HS 1804 + 6753, a new eclipsing dwarf nova of the U Gem class. Its apparent visual brightness in quiescence is $M_\mathrm{V} \approx 14^m$. During its frequent outbursts the brightness increases by $1^m - 2.3^m$. From our photometric data, we determined the orbital period to be $P = 0.2099370^d \pm 0.0000001^d$. The spectroscopic observations show the spectral lines of both stellar components. In quiescence, emission lines of H I, He I, He II, C II, and C III, as well as absorption lines of Fe I, Fe II, Ti II, and O I moving in phase with the primary are visible. During an outburst, additional emission lines of N II, N III, He II, and C III appear. The motion of the secondary can only be derived from a few Ca I absorption lines. The orbital inclination of the system is determined to be $i = (84.2 \pm 0.6)°$. From radial velocities of both components, the respective masses are calculated, yielding $M_1 = (0.75 \pm 0.02)M_\odot$ and $M_2 = (0.56 \pm 0.02)M_\odot$. The mass ratio derived from photometric data confirms the spectroscopic results. The radii of the two components are calculated to be $R_1 = (1.3 \pm 0.1) \cdot 10^{-2} R_\odot$ and $R_2 = (0.57 \pm 0.01)R_\odot$. Several outbursts have been observed so far indicating a relatively high repetition rate.

Key words: stars: binaries: eclipsing – stars: individual: HS 1804 + 6753 – stars: novae, cataclysmic variables

1. Introduction

HS 1804 + 6753 is a new so called double eclipsing cataclysmic binary, which exhibits eclipses of the white dwarf and of the hot spot. It has been detected in the course of the Hamburger Quasar Survey (Bade et al. 1989). The coordinates of this object are $\alpha(2000) = 18^h 04^m 15.1^s$ and $\delta(2000) = 67°54'07''$. A finding chart copied from the Digital Sky Survey is displayed in Fig. 1. HS 1804 + 6753 is a relatively bright CV ($m_\mathrm{V} \approx 14^m$)

in which the eclipse ingress of the white dwarf and of the hot spot are distinguishable. Therefore, the relevant physical parameters of the system can be derived with relatively high precision. Of 800 known cataclysmic binaries, only five exhibit double eclipses. This makes this new CV a fascinating object for extended observations, even more so because it seems to be frequently in outburst. We have monitored HS 1804 + 6753 since April 1991 with telescopes at Wendelstein and Calar Alto collecting spectra as well as high-speed photometric data. Our first results were presented at the IAU symposium 165 (Barwig et al. 1993). Further spectroscopic observations have been reported by Billington et al. (1996).

In Sect. 2, the journal of observations is presented. Data analysing techniques are discussed in Sect. 3 giving masses and radii. In Sect. 4, additional physical parameters are determined by Monte-Carlo techniques.

2. Observation and data reduction

2.1. Spectroscopy

173 spectra were recorded at the Calar Alto Observatory in Spain with the TWIN spectrograph at the 3.5m telescope. During each exposure, a blue and a red spectrum were obtained simultaneously, covering the spectral range between 3440 and 8910Å. For the first observing run in 1992, the GEC#14-CCD (1155∗768 pixel) was used in the blue and the RCA#10-CCD (1024∗640 pixel) in the red range. During this observing run, the system was in quiescence. For the second campaign in 1993, the CCDs were replaced by the TEK#11-CCD and the TEK#12-CCD (both 1024∗1024 pixel), respectively. This time, the system was observed during an outburst. The journal of observations is given in Table 1.

The optimal extraction algorithm given by Horne (1986) was applied to reduce the spectra. This procedure includes the removal of bad pixels and of cosmic ray hits and also takes into account the characteristic bias, the dark current, the pixel-to-pixel-variation, the blaze-function, and the scattered light. For wavelength calibration a helium-argon source was used. This calibration was checked using sky-lines which were superimposed on all exposures. Typical spectra obtained in quiescence and in outburst are displayed in Fig. 2 and Fig. 3. During an outburst, additional emission lines of C II, C III, N III, He I, and
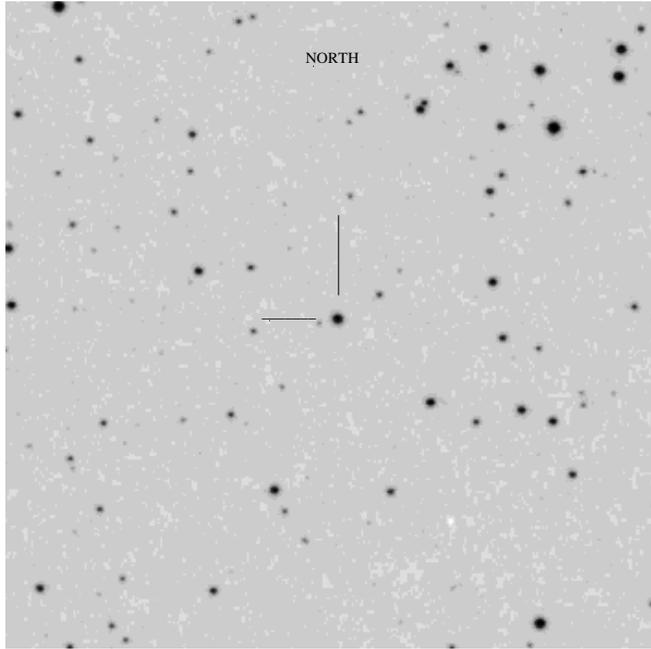
Fig. 1. Finding chart for HS 1804 + 6753, taken from the Digital Sky Survey. The coordinates of the system are $\alpha(2000) = 18^h04^m15.1^s$ and $\delta(2000) = 67°54'07''$. North is up and east is left; scale: 10'x10'.

Table 1. Journal of observations of all spectra. The integration time varies between 200s...1200s.

Date	λ-Range in Å	Dispersion in Å/pixel	No. of spectra / phase range
03/04-07-92	3951...4913	0.84	18 / 0.872-2.195
	6178...6741	0.56	18 / 0.872-2.195
04/05-07-92	3496...5389	1.66	19 / 0.642-1.826
	5686...6812	1.11	19 / 0.642-1.826
05/06-07-92	3441...5335	1.66	12 / 0.442-1.434
	5691...6815	1.11	11 / 0.482-1.434
06/07-07-92	3467...5336	1.66	4 / 0.977-1.128
	5687...6812	1.11	4 / 0.977-1.128
07/08-07-92	3442...5336	1.66	16 / 0.873-1.260
	5689...6813	1.11	16 / 0.873-1.260
19/20-07-93	3838...5628	1.76	1 / 0.874
	6205...8909	2.65	1 / 0.874
20/21-07-93	3836...5628	1.76	15 / 0.701-1.832
	6198...8901	2.65	15 / 0.701-1.832

He II appear between 4700 and 4900Å, as well as the C II emission line at 4262Å and the N II emission line at 6340.67Å. During quiescence, seven Ca I absorption lines in the wavelength range between 6100 and 6500Å are visible which obviously follow the motion of the secondary (Fig. 4). All lines identified in the spectra of HS 1804 + 6753 are compiled in Table 2 to 4 and 7.

Table 2. Emission lines of the primary. Lines which are possibly blended are marked with a 'B'. For the balmer lines and two He lines equivalent widths are given in brackets.

H I	H_α(55.2Å), H_β(35.8Å), H_γ(24.2Å), H_δ(17.6Å), H_ϵ(13.5Å), H_8(11.1Å)
He I	3888(B), 3936(B), 4026, 4102, 4471(6.91Å), 4713(B), 4713, 4922(B), 5016(B), 5876, 6678(5.83Å), 7066
He II	4686(B)
C II	4267
C III	4647...4674(B)
N II	6341
N III	4514(B), 4634...4642(B)
Fe II	4924(B), 5018(B), 5169

Table 3. Absorption lines of the primary.

Fe I	4046, 4132, 4272, 4308(B), 4384, 4405, 4415(B)
Fe II	4417(B), 4550(B)
Ti II	3760(B), 4300, 4308(B), 4315, 4395, 4418(B), 4444, 4501, 4534, 4550(B), 4572(B)
O I	7772...7775(B)

Table 4. Spectral lines of the primary, showing absorption features as well as emission features.

Ca II	3934
Fe II	4233, 4509, 4520(B), 4549, 4584, 4621, 4629, 5235, 5276, 5317(B)

**Table 7.** Absorption lines of the secondary.

Ca I	6103, 6122, 6162, 6439, 6450, 6463, 6494

2.2. Photometry

High-speed simultaneous UBVRI photometry was performed between April 1991 and February 1996 with the 2.2m telescope at Calar Alto and with the 0.8m telescope at Wendelstein Observatory. The total observing time amounts to 330 hours. In all cases the Multichannel-Multicolour Photometer (MCCP) (Barwig et al. 1987) was used. This high-speed photometer consists of three fiber channels so that the program star, a nearby comparison star, and the sky background can be measured simultaneously. Each of the three channels feeds a prism spectrograph in order to split the light into five colours, which nearly fit the Kron Cousins UBVRI photometric standard system. During all observations, the integration time was set to 2 s. The raw data was reduced by applying the standard reduction procedure. For details see Barwig et al. (1987). The journal of observations is listed in Table 5 and 6. Typical UBVRI light curves of HS 1804 + 6753 in quiescence and in outburst are displayed in Fig. 5 and Fig. 6.

Table 5. Journal of the photometric observations (1991-1993). Abbreviations: Observations at Wendelstein: W; Observations at Calar Alto: C; Observations during an outburst: O.

Date of observation	Starttime of measurement (HJD - 2 440 000)	Eclipse egress of the white dwarf and cycle number	Duration (h)	Remarks
24-04-1991	8372.463287	-	3.6	W
26-04-1991	8373.478322	-	2.0	W
21-05-1991	8398.425833	8398.46366 (0)	2.6	W
05-06-1991	8413.361019	8413.36924 (71)	3.0	W
02-07-1991	8440.390694	8440.45112 (200)	4.3	W
04-07-1991	8442.452986	8442.55075 (210)	2.7	W
05-07-1991	8443.357905	-	5.3	W, O
06-07-1991	8444.365301	-	5.0	W, O
07-07-1991	8445.407708	-	1.5	W, O
10-07-1991	8448.391296	8448.42888 (238)	4.1	W
05-09-1991	8505.425486	-	4.0	W
08-09-1991	8508.333912	8508.47163 (524)	7.1	W
09-09-1991	8509.280197	8509.31091 (528)	5.8	W
		8509.52070 (529)		
28-11-1991	8589.459248	8589.50686 (910)	4.6	W
29-11-1991	8590.500127	8590.55629 (915)	4.1	W
12-12-1991	8603.497836	8603.57281 (977)	5.6	W
13-12-1991	8604.495671	-	5.8	W
29-12-1991	8620.440058	-	4.3	W, O
30-12-1991	8621.442188	-	6.2	W, O
31-12-1991	8622.510625	-	4.4	W, O
06-02-1992	8659.567755	-	3.9	W
08-02-1992	8661.480833	8661.51574 (1253)	5.5	W
14-02-1992	8667.366030	8667.60384 (1282)	6.2	W
28-02-1992	8681.315347	8681.45987 (1348)	9.0	W
		8681.66964 (1349)		
29-02-1992	8682.522396	-	4.4	W
01-03-1992	8683.261447	8683.34915 (1357)	7.7	W
		8683.55895 (1358)		
24-05-1992	8767.336192	8767.53386 (1758)	6.2	W
25-05-1992	8768.335972	-	6.0	W
26-05-1992	8769.347280	-	1.1	W
27-05-1992	8770.348831	-	4.2	W
28-05-1992	8771.333380	8771.52288 (1777)	5.5	W
01-07-1992	8805.443993	8805.53289 (1939)	2.6	C
03-07-1992	8807.361875	8807.42219 (1948)	6.7	C
		8807.63229 (1949)		
04-07-1992	8808.366586	8808.47199 (1953)	4.7	C
05-07-1992	8809.420116	-	4.4	C
24-09-1992	8890.518438	8890.55743 (2344)	3.4	W
25-09-1992	8891.278843	8891.39729 (2348)	3.6	W
26-02-1993	9045.488750	-	4.8	W, O
28-02-1993	9047.340104	-	3.0	W, O
02-03-1993	9049.301586	-	1.4	W
08-03-1993	9055.506806	-	4.4	W
14-03-1993	9061.504699	-	4.3	W
19-03-1993	9066.328333	9066.48459 (3182)	6.0	W
20-03-1993	9067.271655	9067.32445 (3186)	7.6	W
		9067.53438 (3187)		
01-04-1993	9079.467616	-	3.8	W
21-07-1993	9190.534306	-	3.0	C, O
22-07-1993	9191.365255	-	3.4	C, O
23-07-1993	9192.580243	-	2.1	C, O
12-09-1993	9243.416979	-	0.2	C
13-09-1993	9244.381111	-	1.7	C
14-09-1993	9245.346262	9245.35032 (4034)	2.0	C
18-12-1993	9340.541667	9340.66163 (4488)	3.6	W
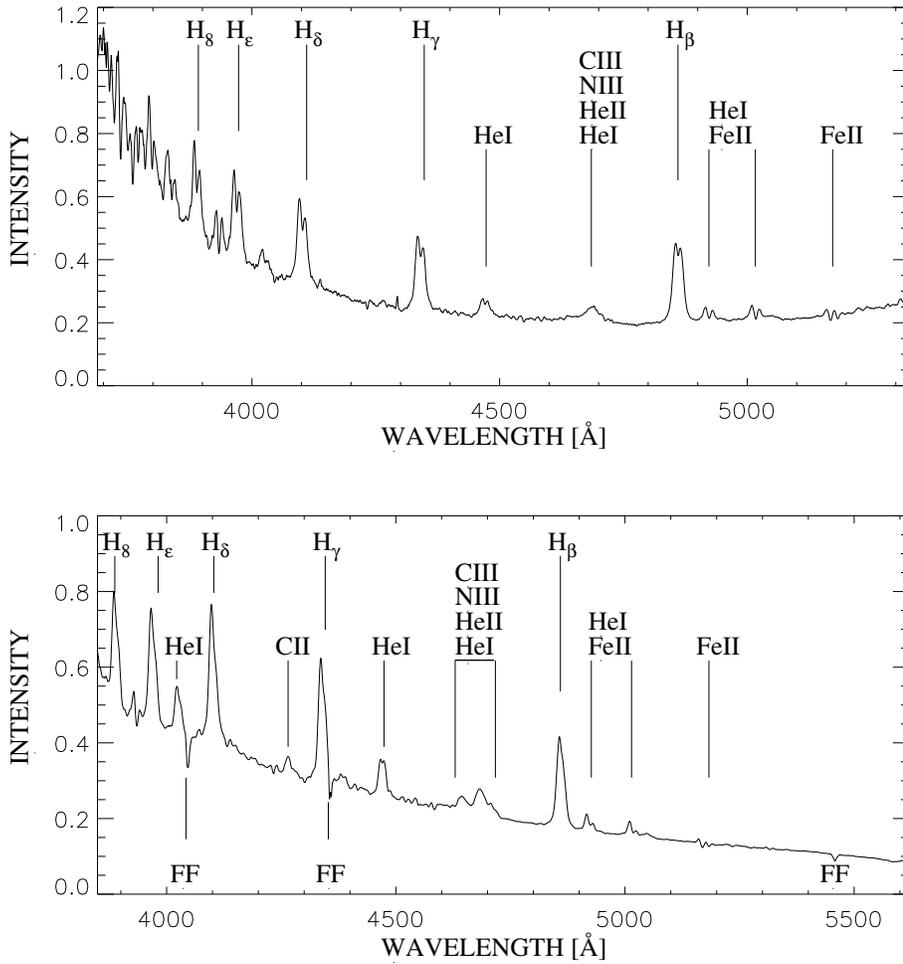
Fig. 2. Blue spectral range of HS 1804 + 6753. Before averaging, the individual spectra were shifted according to the radial velocity $K_1 sin(\phi)$ to emphasize the lines moving with the primary component. The mean spectrum during quiescence is displayed in the upper panel, that during outburst in the lower panel. Dips in the spectra which are caused by emission lines of the flatfield light source are marked with FF. Intensities are given in arbitrary units.

Table 6. Journal of the photometric observations (1996). Abbreviations: Observations at Wendelstein: W; Observations at Calar Alto: C; Observations during an outburst: O.

Date of observation	Starttime of measurement (HJD - 2 440 000)	Eclipse egress of the white dwarf and cycle number	Duration (h)	Remarks
08-01-1996	10091.307616	-	7.4	W
14-01-1996	10097.232859	10097.27450 (8092)	12.0	W
		10097.48439 (8093)		
		10097.69431 (8094)		
15-01-1996	10098.254803	10098.32419 (8097)	11.7	W
		10098.53412 (8098)		
16-01-1996	10099.255637	10099.37389 (8102)	8.9	W
		10099.58383 (8103)		
19-01-1996	10102.229363	-	3.5	W
22-01-1996	10105.384525	-	6.1	W, O
25-01-1996	10108.231470	-	1.2	W, O
28-01-1996	10111.225706	-	5.8	W, O
29-01-1996	10112.239306	-	9.8	W, O
31-01-1996	10114.274340	10114.48934 (8174)	10.8	W
		10114.69943 (8175)		
01-02-1996	10115.229213	-	7.7	W
05-02-1996	10119.233623	10119.31831 (8197)	8.2	W
		10119.52791 (8198)		
06-02-1996	10120.226331	10120.36766 (8202)	10.8	W
		10120.57775 (8203)		
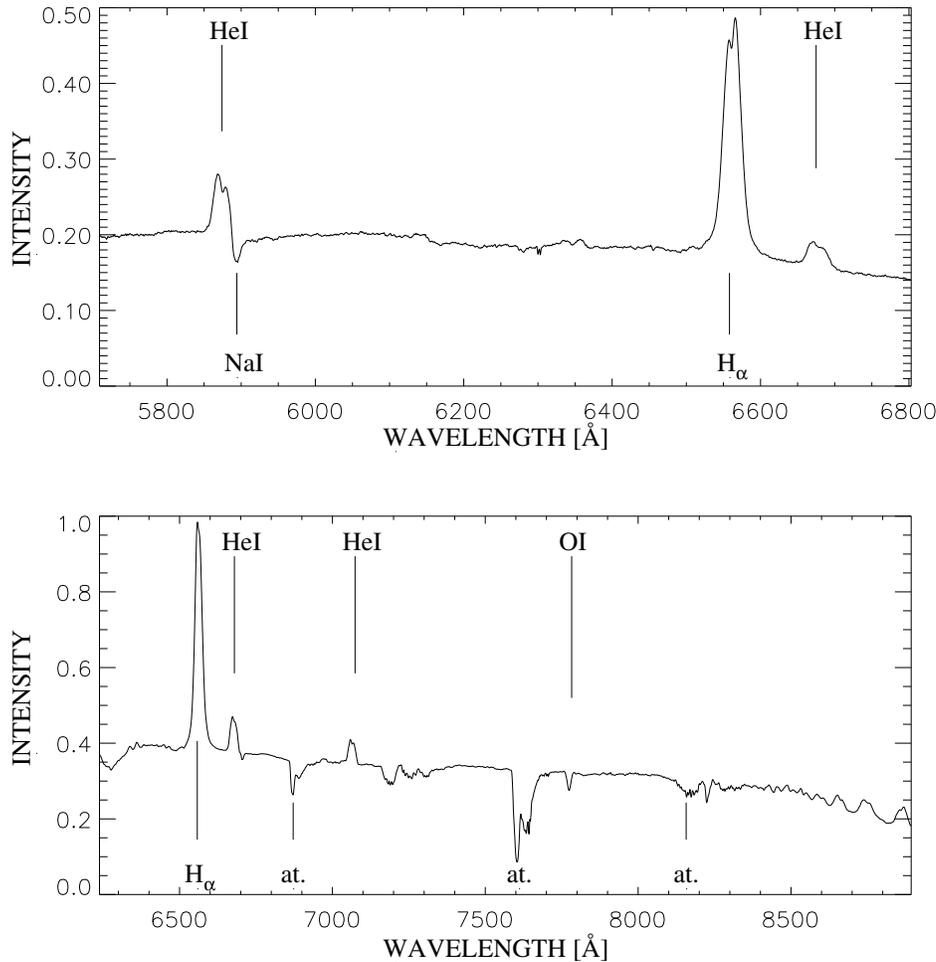
Fig. 3. Red spectral range of HS 1804 + 6753. Before averaging, the individual spectra were shifted according to the radial velocity $K_1 sin(\phi)$ to emphasize the lines moving with the primary component. The mean spectrum during quiescence is displayed in the upper panel, that during outburst in the lower panel. Atmospherical absorptions are marked with "at." . Intensities are given in arbitrary units.

3. Data analysis

3.1. Photometry

3.1.1. Period analysis

The characteristic eclipse features of HS 1804 + 6753 are displayed in Fig. 7, which are applied to derive the orbital period. The phase points Φ_1 and Φ_4 indicate ingress and egress of the hot spot, Φ_2 and Φ_3 that of the white dwarf. The most stable well-defined eclipse feature is the mid egress of the white dwarf. During the eclipse ingress additional light from the hot spot may disturb the light curve. The exact mid egress time is determined by fitting an approximating spline to each of the light curves and by calculating their derivatives. At the mid egress of the white dwarf, the derivative shows a local maximum, which gives the mid egress time with an accuracy of 4 s. Assuming that the orbital period is constant over the observation period, we derived its value by fitting a straight line through these points. Since we know the duration of the eclipse of the white dwarf (see Sect. 3.1.2), the ephemeris of its mid eclipse time T_0 is calculated to

$$T_0 = \text{HJD} \quad 2448398.452908^d + 0.2099370^d \cdot E \qquad (1)$$
$$\pm 0.000003^d \pm 0.0000001^d$$

The measured eclipse timings and their corresponding cycle numbers are given in Table 5 and 6. However, from a plot showing residual vs cycle-number (Fig. 8), the orbital period does not seem to be constant. This may be caused by some unknown distortion of the eclipse egress or by a shift of this feature indicating real period changes. In this case, possible explanations include influence by a third body in the system or, more likely, magnetic activity of the secondary star (Warner, 1988). Similar period fluctuations on time scales of years have been observed e.g. for IP Peg (Wolf et al., 1993).

3.1.2. Eclipse times

In order to separate the eclipse of the hot spot from that of the white dwarf a mean light curve was derived from the data using the ephemeris given in Eq. (1). The mean B light curve together with its derivative are plotted in Fig. 7. Due to the temperatures of both the hot spot and the white dwarf and due to the λ-dependent quantum efficiency of the detectors, the B channel provides a maximum signal-to-noise ratio. The local extrema of the derivatives taken from the B channel give the four phase points $\phi_1 \ldots \phi_4$

$$\phi_1 = -0.060424 \pm 0.000047$$
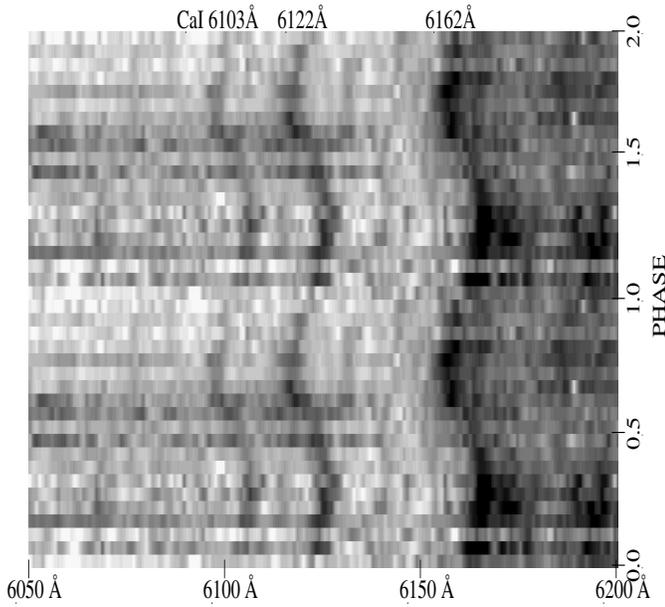
Fig. 4. Radial velocity variations of the Ca I absorption lines of the secondary component. 20 spectra are arranged in sequence of increasing orbital phase. The phase interval is repeated for clarity.

$\phi_2 = -0.055131 \pm 0.000047$

$\phi_3 = 0.055131 \pm 0.000047$

$\phi_4 = 0.097803 \pm 0.000047$

ϕ_3 defines the mid egress of the white dwarf, while ϕ_4 defines that of the hot spot. The small error bars are due to superposition of 50 light curves, assuming again the orbital period to be constant. The duration of the white dwarf's egress can not be measured due to considerable radiation from the disk. Nevertheless, this does not affect the determination of the mid egress. In principle, in order to assign the ingress phase points ϕ_1 and ϕ_2 to the respective components, two methods can be applied. During an outburst most of the optical radiation originates from the disk. Assuming a symmetrical disk, its eclipse should be symmetrical to the mid eclipse of the white dwarf. Thus, from the observed mid eclipse time during an outburst and from the observed mid egress time during quiescence, the mid-ingress time of the white dwarf can be calculated. However, this method can not be applied to HS 1804 + 6753 since the eclipse light curve is asymmetric in outburst (see Fig. 6). On the other hand, an ingress/egress phase diagram can be used together with a single particle trajectory (SPT) to determine the position of the hot spot. As shown in Sect. 3.1.3 a unique solution can be found if the hot spot is eclipsed first. Therefore, the duration between mid ingress and mid egress of the hot spot Δt_{HS} and that of the white dwarf Δt_{WD} is

$$\Delta t_{WD} = (2000 \pm 9)\text{s} \qquad (2)$$
$$\Delta t_{HS} = (2870 \pm 9)\text{s} \qquad (3)$$

with a time difference δt of the mid eclipses

$$\delta t = (339 \pm 9)\text{s} \qquad (4)$$
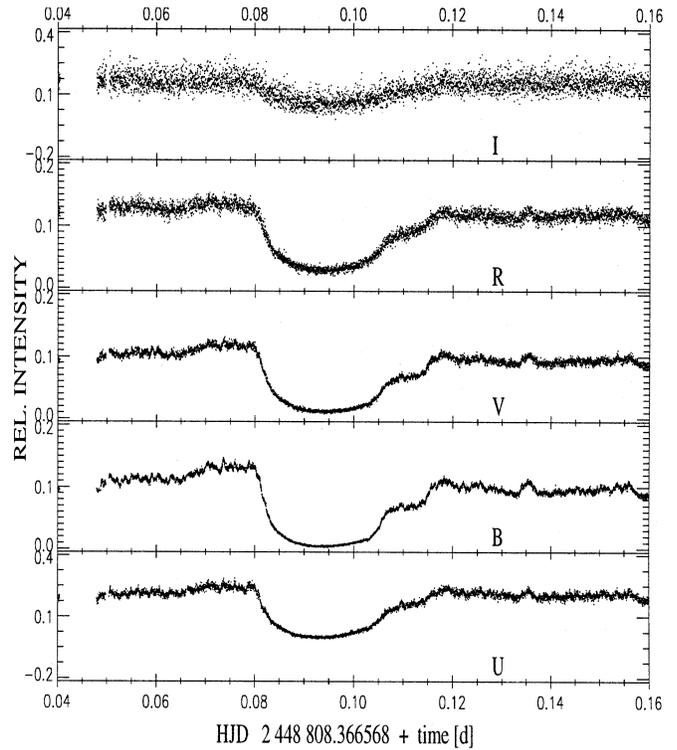
Fig. 5. Typical UBVRI light curves of HS 1804 + 6753 during quiescence measured relative to a comparison star. The photometric data were recorded with the MCCP at Calar Alto Observatory on 4.7.1993. Each data point represents an integration of 2s.

3.1.3. Photometric mass ratio

The mass ratio $q = M_2/M_1$ of the components of HS 1804 + 6753 was calculated from their respective radial velocities. The value of the mass ratio is confirmed by solving the SPT under the influence of the Roche potential (Dreier, 1986). This photometric method yields solutions for the SPT assuming that the hot spot is eclipsed first. Different SPTs fitting the equations yield mass ratios between 0.7 and 0.8 in close correspondence with the spectroscopic results (Fig. 9).

3.2. Spectroscopy

3.2.1. Radial velocity of the white dwarf

The radial velocity of the white dwarf is derived from spectra observed during quiescence. For the determination of the velocity K_1 the double-peaked emission lines of H_β, H_γ, and H_δ were taken. Radial velocities derived from other emission lines turned out to be less reliable. Line profiles were measured applying the method of Schneider and Young (1980). This method employs two Gaussian bandpasses, specified by their FWHM σ and separation a, to measure the wings of the emission line, finding the velocity shift required to make the line flux equal in the two bandpasses. This yields different K_1 values as a function of these two parameters. The calculated velocities can be
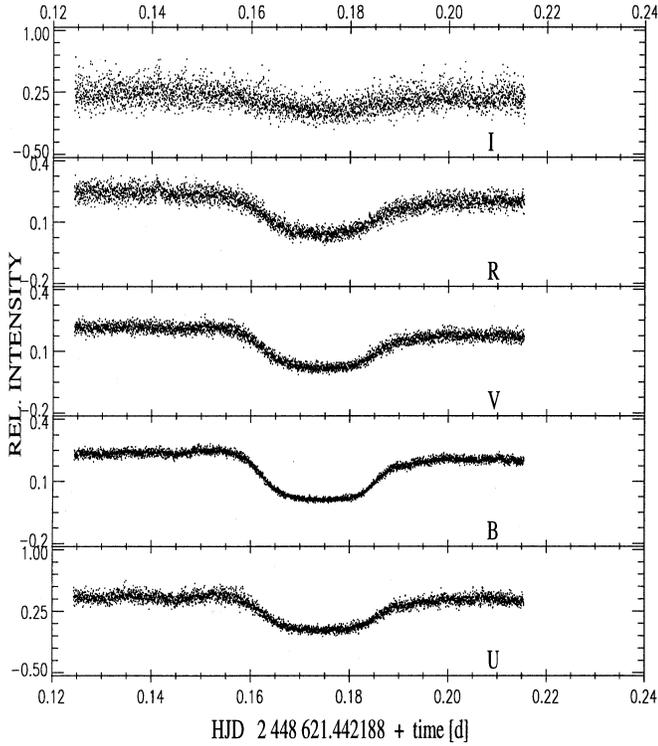
Fig. 6. Typical UBVRI light curves of HS 1804 + 6753 during outburst measured relative to a comparison star. The photometric data were recorded with the MCCP at Wendelstein Observatory on 30.12.1991. Each data point represents an integration of 2s.

fitted by the equation

$$V = \gamma - K_1 \sin(\varphi - \varphi_0) \qquad (sin(i) \approx 1) \qquad (5)$$

with γ = system velocity

K_1 = amplitude of the velocity of the white dwarf

φ = phase of the system

φ_0 = phase shift of the system

The value with a minimal relative error, σ_{K_1}/K_1 is selected (Fig. 10). From this, the weighted mean radial velocity for the white dwarf is derived to

$$K_1 = (167 \pm 3)\text{km/s} \qquad (6)$$

Note that possible systematic errors have not been considered.

3.2.2. Radial velocity of the secondary

The sole spectral signatures of the secondary are absorption lines of Ca I. In order to derive their radial velocities, Gaussian profiles were fitted. The value of K_2 was calculated from

$$V = \gamma - K_2 \sin(\varphi - \varphi_0) \qquad (\text{see } (6)) \qquad (7)$$
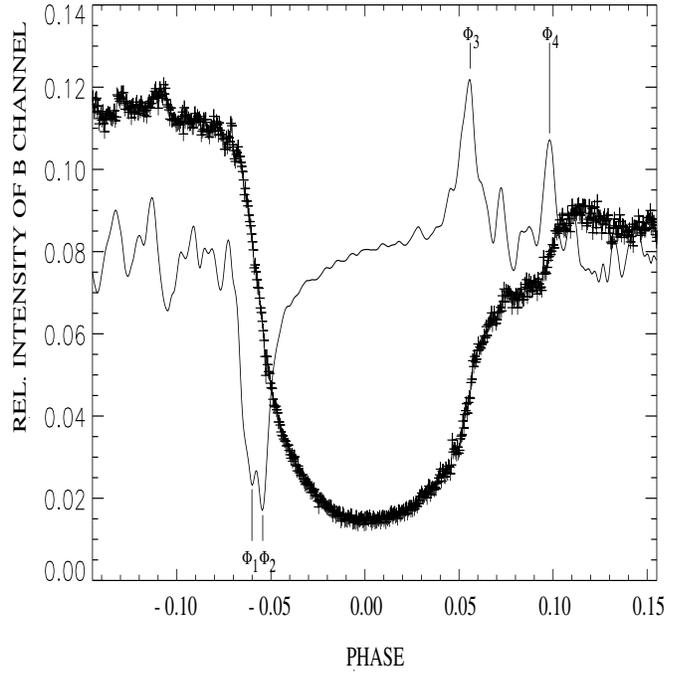
Fig. 7. Mean B light curve (crosses) and its corresponding derivative (solid line). The mid ingress and mid egress times of the hot spot (Φ_1, Φ_4) and of the white dwarf (Φ_2, Φ_3) are marked.

The resulting phase shift is nearly zero. This is consistent with the assumption that the photocentre of the secondary coincides with its mass centre. The weighted radial velocity obtained from 266 line profiles (Fig. 11) is

$$K_2 = (223 \pm 1)\text{km/s} \qquad (8)$$

Note again that systematic errors have not been considered.

3.2.3. System velocity

The system velocity is derived from the radial velocity curves of the two components. A sine-fit through both velocity curves yields

$$\gamma_1 = -(26.4 \pm 1.8)\text{km/s}$$
$$\gamma_2 = -(29.7 \pm 0.9)\text{km/s}$$

4. Determination of system parameters

In this section, the masses M_1 and M_2, the radii R_1 and R_2, the inclination i, the distance a of the two stars, the distance f of the inner Lagrangian point L_1 from the white dwarf, and the radius d of the disk in quiescence are calculated. First, the applied formulas are explained, then the parameters are calculated and discussed.
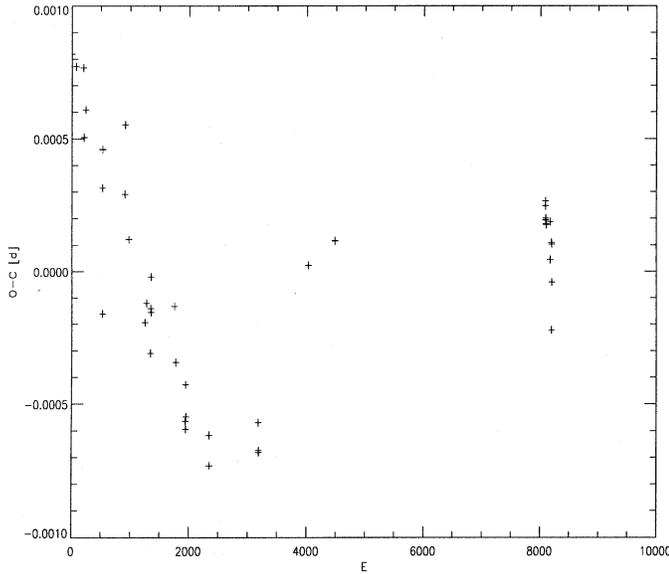
Fig. 8. O-C residuals of the eclipse egress times of the white dwarf calculated from the ephemeris given in Eq.(1).

4.1. Functional context

The mass ratio $q = M_2/M_1$ can be described by the radial velocities

$$q = \frac{K_1}{K_2} \tag{9}$$

For the calculation of the inclination i we applied the LFIT code (Wolf et al, 1995), keeping the q-value calculated above. This code decomposes eclipse light curves by fitting an N-component light curve model to the observational data. In this case, the model light curve is subdivided into 4 components: The white dwarf, assumed to be a spherical object with radius R_1; the secondary depending on the mass ratio q and the inclination i, assuming Roche-geometry; the accretion disk, represented by the disk radius d and a radial intensity distribution; and last, the hot spot.

Furthermore, Kepler's third law combined with an empirical equation of Paczynski (1971)
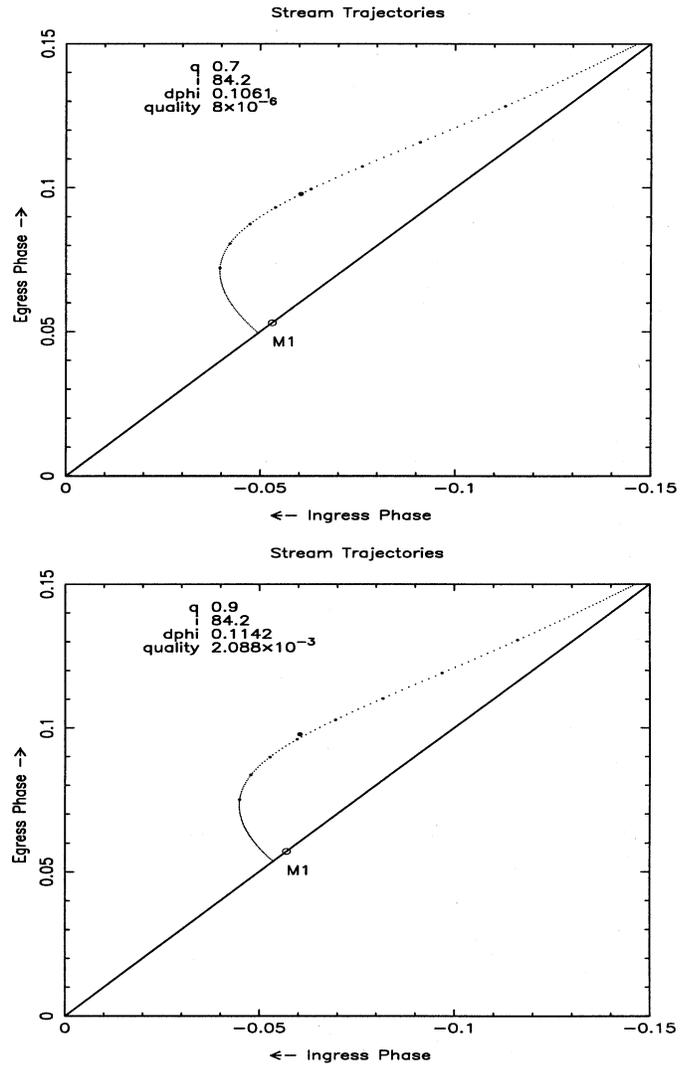
$$\frac{R_2}{a} = \frac{2}{3^{4/3}} \left(\frac{q}{1+q} \right)^{1/3} \tag{10}$$

yields a mass-radius relation of the secondary as a function of the orbital period P

$$M_2 = \frac{81\pi^2}{2G} \frac{1}{P^2} R_2^3 \tag{11}$$

with the gravitational constant G. The relative distance f of the inner Lagrangian point L_1 from the white dwarf only depends on the mass ratio q (Warner, 1976; Plavec, 1964)

$$\frac{f}{a} = 0.500 + 0.227 \cdot \log q \qquad \text{for } 0.1 \leq q \leq 10 \tag{12}$$

Fig. 9. Different trajectories for mass ratios 0.5 . . . 1.0. The hot spot is identified by the dot at (-0.55131/0.097803).

For the white dwarf, the mass-radius relation of Nauenberg (1972) is applied

$$\frac{R_1}{R_\odot} = 1.125 \cdot 10^{-2} \sqrt{\left(\frac{M_1}{1.44 \cdot M_\odot} \right)^{-2/3} - \left(\frac{M_1}{1.44 \cdot M_\odot} \right)^{2/3}} \tag{13}$$

4.2. Calculation of the parameters

The parameters and their corresponding errors are calculated by a Monte-Carlo simulation. For this, 10 000 Gauss-distributed starting-values of K_1 and K_2, and the orbital inclination i derived by the LFIT code are simulated. The error of the period is neglected. Assuming Roche geometry, the starting-values are taken and the following parameters are calculated together with their standard deviations:

- Mass ratio $q = 0.75 \pm 0.01$
- Inclination $i = 84.2° \pm 0.6°$
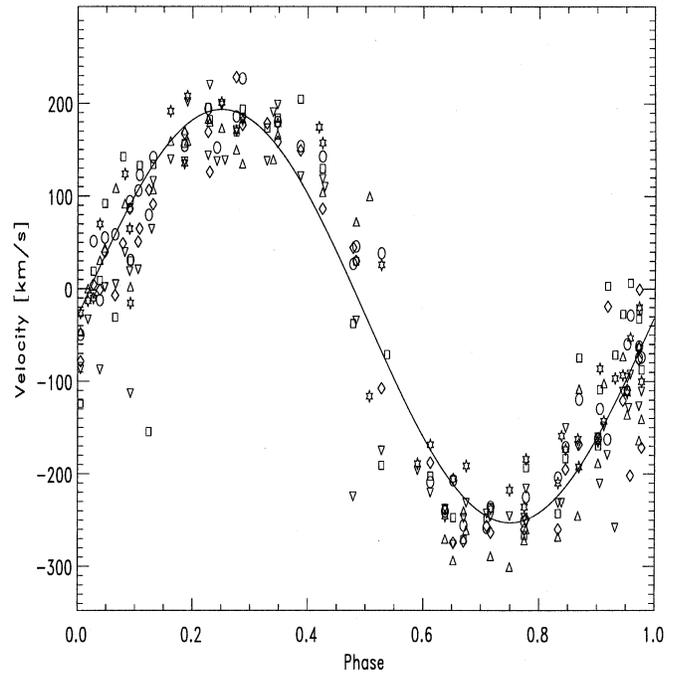- Distance f in units of a: $f/a = 0.471 \pm 0.002$
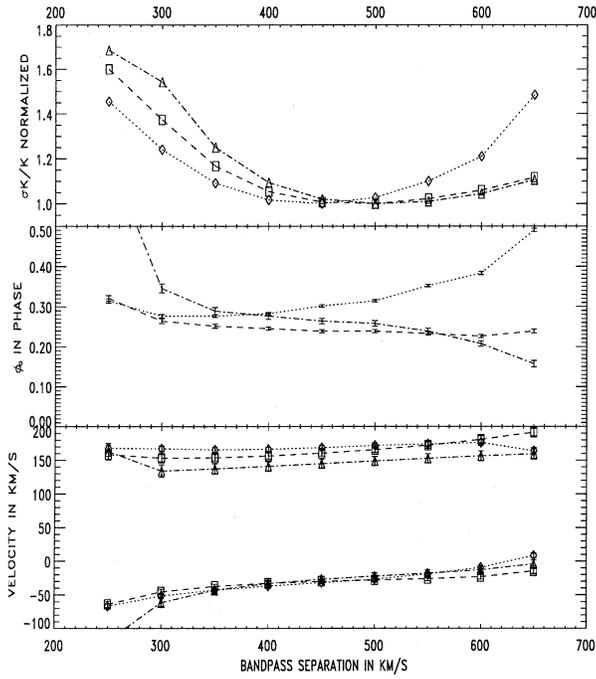
Fig. 10. K_1 velocities vs bandpass separation and their respective system velocities γ (upper panel). H_β is marked with a $\diamond$, H_γ with a $\square$, and H_δ with a $\triangle$. In the middle panel their respective angles ϕ are plotted, and in the lower panel the minimal relative error σ_{K_1}/K_1 is shown.

Fig. 11. Radial velocity curve of the secondary component measured from the following absorption lines: Ca I 6103Å ($\square$), Ca I 6122Å ($\diamond$), Ca I 6162Å ($\circ$), Ca I 6439Å ($\triangledown$), Ca I 6450Å ($\triangle$), Ca I 6463Å ($\bar\triangledown$) For clarity error-bars have not been plotted.

- Distance $a = 1.63 R_\odot \pm 0.02 R_\odot$
- Mass $M_1 = 0.75 M_\odot \pm 0.02 M_\odot$
- Mass $M_2 = 0.56 M_\odot \pm 0.02 M_\odot$
- Radius $R_1 = 0.013 R_\odot \pm 0.001 R_\odot$
- Radius $R_2 = 0.57 R_\odot \pm 0.01 R_\odot$
- Relative mean radius of the disk in quiescence $d/a = 0.27 \pm 0.01$

5. Discussion

Cataclysmic binaries are most efficient for the investigation of accretion processes on short time scales. To understand the dynamics of accretion phenomena, the parameters of the interacting components in a CV system must be sufficiently well known. These parameters can only be derived with high precision from eclipsing binaries in which the eclipse of the hot spot and that of the white dwarf can be measured separately and radial velocity curves of both components are available. At present, only five systems fitting the required characteristics are known. HS 1804 + 6753 has proved to be a new member of this class. In this paper, relevant system parameters of HS 1804 + 6753 are given. Their relatively small errors are due to the large number of measurements involved. So far, systematic errors have not yet been considered. They may occur when measuring the radial velocities of the stellar components.

For the secondary, there is no phase shift between the mid eclipse determined from the observed radial velocity curve of the secondary and the white dwarf's ingress and egress timings calculated from the photometric data. Hence, it is assumed that for this component the mass centre and the photocentre coincide. This indicates that the heating of the secondary by the primary can be neglected.

However, for the white dwarf a phase shift of $\Delta\Phi = 0.044 \pm 0.002$ is observed. This phenomenon may be due to an asymmetrical disk or an excentric photocentre of a symmetrical disk, e.g. caused by the hot spot (Marsh, 1988). Nevertheless, the derived photometric mass ratio coincides with the spectroscopic one. A possible influence of the phase shift on K_1 seems to be negligible, as proved by the coincidence of the photometric and spectroscopic mass ratio. Furthermore, the similarity of the derived system velocities γ_1 and γ_2 indicates that there are probably no relevant distortions of the line profiles.

The location of the hot spot itself is dependent on the radius of the disk, and therefore depends on the activity state of the system. From a superposition of different eclipse light curves in quiescence, only a mean radius could be derived. The observed fluctuations of the eclipse egress of the white dwarf and the resulting possible period fluctuations are too small to affect the derived physical parameters.

In all calculations, the secondary is not assumed to be a lower main sequence star. This can now be proved by applying the mass-radius relation of Patterson (1984)

$$\frac{R}{R_\odot} = \frac{M}{M_\odot}^{0.88 \pm 0.02} \qquad \text{for} \quad 0.1 \leq \frac{M}{M_\odot} \leq 0.8 \quad . \qquad (14)$$

For $M_2 = 0.59 M_\odot$ a radius of $R_{Patterson} = 0.62 \ldots 0.63 R_\odot$ is calculated. Therefore, the secondary star is definitely not above the main sequence and therefore not evolved.

In principle, from the radiation and the spectral type of the secondary the distance of HS 1804 + 6753 can be derived. Its spectra are preferably taken during the eclipse of both the white dwarf and the hot spot. Even during this phase interval, the observed S/N of the spectra are too low to derive the true spectral type. The only spectral signature of the secondary are Ca I absorption lines, no TiO bands could be detected (see Table 7). The relative ratios of these lines indicate a spectral type of M0, although the spectrum of the secondary is contaminated with that of the accretion disk throughout the eclipse.

The origin of the Ti II absorption lines showing the motion of the primary component is still unknown. Their equivalent widths obviously increase towards the blue spectral range. It must be proved whether they originate from the disk or from the white dwarf itself.

Furthermore, HS 1804 + 6753 is an interesting object because of its frequent outbursts. Normally, the amplitude of an outburst does not exceed 1^m, which is lower than expected for dwarf novae, but outbursts up to 2.3^m have been recorded. During an outburst the hump apparently disappears and a U-shaped eclipse feature appears. For yet unknown reasons, the slope of the egress feature is steeper than that of the ingress. However, the minimum brightness during the eclipse drops to the same level in quiescence as well as in outburst, indicating that the source of the outburst is totally eclipsed by the secondary. From light curves taken during different outbursts, an investigation of the dynamic behaviour of the accretion disk is expected.

Further investigations of HS 1804 + 6753 will include spectral eclipse-mapping as well as Doppler-tomography to reveal e.g. the origin of the Ti II absorption lines. Due to the relatively high precision of the derived system parameters and the obviously high outburst frequency, HS 1804 + 6753 appears to be an outstanding system for the analysis of the involved accretion phenomena.

References

Bade N., Hagen H.-J., Reimers D., 1989, 23 Eslab Symp. ESA SP-296, p.883
Barwig H., Fiedler H., Reimers D.,Bade N., 1993, in van Woerden H., ed., Abstracts of IAU Symp. 165, Compact Stars in Binary Systems, p.89
Barwig H., Schoembs R., Buckenmayer C., 1987, A&A 175, 327
Billington I., Marsh T.R., Dhillon V.S., 1996, MNRAS 278, 673
Dreier H., 1986, Diplomarbeit at the Universitătssternwarte Műnchen
Horne K., 1986, Astron. Soc. of the Pacific, 98, 609
Marsh T.R., 1988, MNRAS 231, 1117
Nauenberg M., 1972, ApJ 175, 417
Paczynski B., 1971, ARA&A 9, 183
Patterson J.P., 1984, ApJS 54, 443
Plavec M., 1964, Bull. of the Astron. Inst. of Czechoslovakia, 15, 165
Schneider D.P., Young P., 1980, ApJ 238, 946
Warner B., 1976, IAU Symposium Nr. 73
Warner B., 1988, Nat 336, 129
Wolf S., Mantel K.H., Horne K., 1993, A&A 273, 160
Wolf S., Horne K., Marsh T.R., 1995, Science with the Hubble Space Telescope - II, eds. P. Benvenuti, F.D. Macchetto, E.J. Schreier, p. 424